these activation energies take on a somewhat more involved interpretation.

ACKNOWLEDGMENTS

Theory of Dislocation Mobility in Semiconductors*

V. Celli,† M. Kabler,‡ T. Ninomiya and R. Thomson
Department of Metallurgy, University of Illinois, Urbana, Illinois
(Received 11 February 1963)

A new model for dislocation motion appropriate for crystals having high Peierls stress is presented. The model makes use of dragging points on the dislocation which restrict the free motion of kinks on the line. It predicts a dislocation velocity with an exponential dependence inverse in the stress and an activation energy appropriate to kink nucleation. In extensive Appendixes, kink theory is used to develop explicit formulas for the stress dependence of the kink nucleation energy and to work out the statistical details of the nucleation rate. Also, a detailed theory of kink collisions is developed when the kink population is high. Finally, the experiments of Kabler described in the previous paper of this journal are interpreted in terms of the model with appropriate parameters for Ge.

I. INTRODUCTION

THE mobility of individual dislocations as a function of stress and temperature has been measured by etch-pit techniques for several non-metals.[1-3] In all cases the mobility increases rapidly with temperature, consistent with the idea that the dislocation motion is thermally activated. If the resistance to motion were simply due to the interaction of the dislocation strain field with thermal vibrations, the mobility should decrease with temperature.[4] Thus, the dislocation does not behave as if it were moving in a homogeneous elastic continuum, and other possible obstacles to motion must be considered.[5] These can be due to the discrete nature of the crystal medium (Peierls barrier), or to the interaction of the dislocations with other defects or impurities present in the material. Furthermore, it is well known that jogs on screw dislocations cannot glide conservatively, at least when they are several Burgers vectors high. Thus, the drag on the dislocation due to debris formation must also be considered.

The various mechanisms mentioned above are not mutually exclusive, and it is often difficult to decide which one is the most important in a given material.

In the case of LiF it has been shown that the divalent impurities present in the crystal can provide a drag of the observed order of magnitude,[6,7] and that vacancy trails due to nonconservative jogs can explain the difference between the mobility of screw and edge dislocations. There is no evidence of an important Peierls energy in this case.

On the other side in the semiconductors, germanium and silicon, evidence of formation of vacancy trails has been found both for screw and 60° dislocations,[8] but a simple calculation shows that at stress levels where the dislocation velocity is only about 10^{-3} cm/sec, the work done by the applied stress is large enough to create one point defect of energy 1 eV every ten atoms along the dislocation per every Burgers vector traversed by the dislocation line.[9] Such a high defect formation rate is unreasonable without direct supporting evidence. A similar argument can be applied to the drag exerted by impurities present in the lattice.

It has been commonly supposed that the Peierls energy in the diamond lattice is high, and glide dislocations have been observed in these crystals to lie straight along crystallographic directions. This result can hardly be explained without the existence of a

[1] W. G. Johnston and J. J. Gilman, J. Appl. Phys. **30**, 129 (1959).
[2] A. R. Chaudhuri, J. R. Patel, and L. G. Rubin, J. Appl. Phys. **33**, 2736 (1962).
[3] M. N. Kabler, preceding paper, Phys. Rev. **130**, 54 (1963); hereafter referred to as I.
[4] G. Leibfried, Z. Physik **127**, 344 (1950); see also, J. Lothe, Phys. Rev. **117**, 704 (1960).
[5] A. H. Cottrell, *Dislocations and Plastic Flow in Crystals* (Clarendon Press, Oxford, 1953).
[6] W. G. Johnston, J. Appl. Phys. **33**, 2050 (1962).
[7] R. L. Fleischer, J. Appl. Phys. **33**, 3504 (1962).
[8] W. C. Dash, J. Appl. Phys. **29**, 705 (1958).
[9] If, typically, the Burgers vector is $b=4$ Å and the resolved shear stress is $\tau=25$ kg/mm², then $\tau b^3 = 0.1$ eV.

large Peierls energy.[10] This is also consistent with the apparently intrinsic hardness and fragility of these materials up to several hundred degrees Centigrade. However, a theory of dislocation mobility based only on the Peierls energy fails to give the correct stress dependence of the dislocation velocity; this point is discussed in more detail in Sec. II. We are then led to consider the more complex model described in Sec. III. The primary physical assumption on which our model rests is that, while the dragging force is mainly due to the existence of Peierls barriers, the presence of discrete dragging points effectively restricts kink nucleation to the longer free segments of the line. The nature of the dragging points need not be specified; they could be nonconservative jogs or impurities present in the lattice or highly stable arrangements of bonds in the core of the dislocation. A comparison of the formulas obtained with the data of Kabler[3] on germanium is given in Sec. IV and the nature of the dragging points is discussed for this case.

In the main text of this paper, the argument presented revolves around the general character of kinks on the dislocation, and does not require specific knowledge of the core structure of the dislocation, or of the statistics of kink creation and annihilation. However, in the comparison of the general theory with experiment, it becomes useful to make more detailed guesses about the particular structure of kinks. Therefore, in several extended Appendixes, we have carried out more elaborate theoretical calculations, using specific models. Appendixes A and B pertain to the static and dynamic structure of the flexible string model of a kinked dislocation, and Appendix D considers the problem of kink collisions on a dislocation with randomly spaced segments.

II. PEIERLS BARRIER AND KINK NUCLEATION

The atomic configuration in the core of a gliding dislocation changes continuously as the dislocation moves through the crystal. It is essential for a theory of glide in an ideal crystal to be able to describe these configurations and calculate the partition sum in their neighborhood in phase space. However, the best we can do from first principles at present is to estimate the energies E_I and E_{II} of the stable and unstable equilibrium configurations of a straight dislocation in the absence of applied stress.[11] The difference $E_{II} - E_I$ is the Peierls energy barrier. The Peierls stress, defined as the minimum stress necessary to move a straight dislocation in a perfect crystal, has no simple relation to the Peierls energy and should be calculated by solving the problem of the equilibrium of a dislocation in a crystal under stress. Less rigorously, we can draw
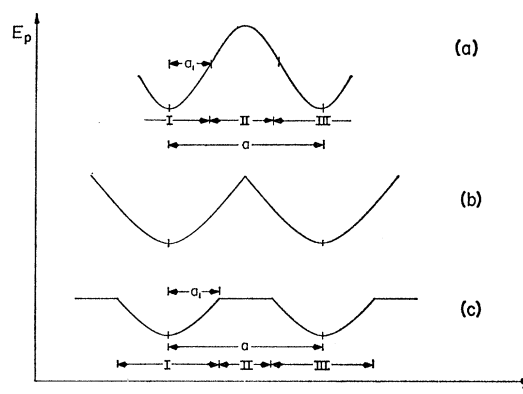

FIG. 1. The energy of a straight dislocation as a function of position in the lattice. The Peierls energy is the difference between maximum and minimum energy values. Three simple types of energy functions are shown. (a) The energy is parabolic with upward concave parabola at I and III and a downward concave parabola at II. The parabolas meet at a_1 with continuous slope. The distance between Peierls troughs is a. (b) The energy is a set of equal cusped parabolas. (c) The energy is a set of parabolas separated by constant energy sections. This case corresponds to the extreme "broken bond" model of a moving dislocation. Analysis using these three types of energy functions is presented in the Appendixes.

a reasonable energy profile between the configurations I and II (see Fig. 1) and assume that the Peierls stress is given by the maximum slope of this profile. Whether this assumption and the concepts of Peierls energy and stress themselves are justified has been discussed in detail recently[12] and the conclusion seems to be positive for the covalent crystals in which we are interested.

To proceed further, we must make the stronger assumption that for small deviation from a straight line the dislocation can be described as a string having a tension constant E_0 of the order of the core energy per unit length. We are interested in finding the energy necessary to make a dislocation bulge over from one Peierls valley into the next as in Fig. 2. This configuration of the dislocation line is called a double kink consisting of a left-side and a right-side kink. For a critical width x^* of the double kink there will be a saddle point in the configurational energy of the dislocation. In Appendix A we indicate how to calculate the energy E at the saddle point as a function of the applied stress τ and give $E(\tau)$ explicitly for the simple Peierls energy potentials sketched in Fig. 1. The
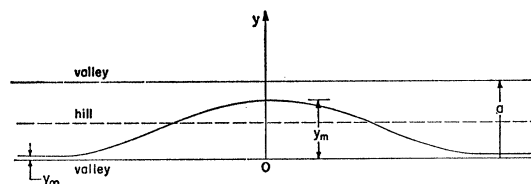

FIG. 2. A dislocation kink pair. The dislocation is represented as a flexible string with displacement $y(x)$.

[10] W. C. Dash, *Dislocations and Mechanical Properties of Crystals* (John Wiley & Sons, Inc., New York, 1957), p. 57. See also Kabler, I.

[11] V. Celli, J. Phys. Chem. Solids **19**, 100 (1961).

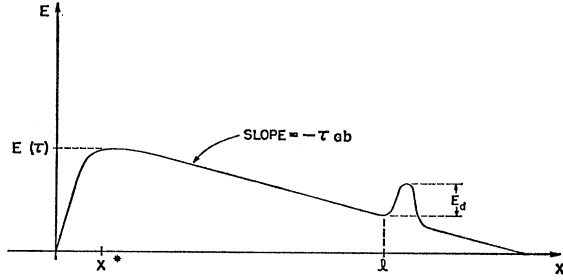[12] Doris Kuhlman-Wilsdorf, Phys. Rev. **120**, 773 (1960).

FIG. 3. Energy of a kink pair as a function of the pair separation in an external stress field. x^* is the saddle-point separation, l is the distance between the first pinning points, and E_d is the pinning-point barrier.

magnitude of $E(\tau)$ agrees with the results of previous treatments (see Sec. IV) in which the applied stress was not exactly taken into account,[13] but the stress dependence is slightly different.

If only the Peierls barrier opposed dislocation motion, we would obtain for the dislocation velocity a formula of the type

$$v = v_0 \exp[-E(\tau)/kT], \qquad (1)$$

with v_0 essentially stress-independent.[14] That such a formula cannot possibly fit the experimental data can be seen by comparing Figs. 4 and 5 of I with the expressions for $E(\tau)$ given in (A9), (A11), and (A12b). It is seen that the function $\ln(v/v_0)$ vs $\ln\tau$ is found experimentally to be concave downwards, whereas the theoretical expressions for $E(\tau)$ give functions which are concave upwards, except for stresses close to the Peierls stress, where the model is highly questionable anyhow. It is seen that if we put

$$E(\tau) = E^* - \tau bax^*, \qquad (2)$$

where a is the kink height and b the Burgers vector, x^* turns out to be only slowly stress-dependent and can be regarded as constant. It is natural to identify x^* with the critical width of the double kink at the saddle point.

There is a possibility that a detailed analysis of the thermal nucleation process of a double kink in the presence of applied stress may show that, in Eq. (1), v_0 does actually depend strongly on τ. Such an analysis is carried out in Appendix B where the nucleation rate of double kinks on the dislocation is given by Eqs. (B19) and (B20), and (B23) and (B24). The stress dependence is in the wrong direction.

In the above discussion, we have neglected the long-range elastic strains associated with the dislocation, under the assumption that we are really dealing with rearrangements of the core structure. The elastic theory of dislocations has been applied to the calculation of the energy of a double kink by Kroupa and

[13] A. Seeger, Phil. Mag. 1, 651 (1956); H. Donth, Z. Physik 149, 111 (1957).
[14] J. Lothe and J. P. Hirth, Phys. Rev. 115, 543 (1959).

Brown.[15] They find that the elastic self-energy of the two constituent kinks vanishes and loses meaning if the kink height a is smaller than a few core radii. However, the expression for the interaction energy of the two kinks remains meaningful for small kink height and is given by

$$E_{el} = -(Gb^2/8\pi)(a^2/r), \qquad (3)$$

where G is an appropriate combination of the elastic constants and r is the kink separation. If we were to keep only this elastic interaction, the energy of the double kink would be $E^* - \tau bar + E_{el}$ and the saddle-point energy would be

$$E(\tau) = E^* - 2\tau^{1/2}(Gb^3a^3/8\pi)^{1/2}. \qquad (4)$$

Inserting (4) into (1) does not alter the qualitative disagreement between the theoretical and experimental stress dependence of the velocity discussed above, and we might expect that the same conclusion would hold if a combined treatment of elastic and core effects were attempted. We then need to include something else in the picture in either case.

III. A NEW MODEL OF DISLOCATION GLIDE

Consider a long straight dislocation lying initially in a Peierls potential valley and suppose that the dislocation is divided into a number of segments by randomly distributed identical dragging points. We do not discuss at this point the nature of these dragging points, except to assume that they offer a barrier to the spreading of a double kink as depicted in Figs. 2 and 3 and remain with the line in a random distribution during glide. When a double kink is nucleated on a free segment of length l between two dragging points, the potential energy of the configuration, as a function of the distance x between kinks, can be schematically drawn as in Fig. 3. Let $\nu^*(l)$ be the rate at which double kinks are created on the segment under consideration. As shown in Appendixes A and B, Eq. (B.20),

$$\nu^*(l) = (l/a)\nu_0^* e^{-E(\tau)/kT}. \qquad (5)$$

After nucleation, the kink pair expands freely until it comes against the dragging points. The work done by the applied stress τ in this expansion is $\tau ba(l-x^*)$. Then the probability per unit time that a double kink (stopped at width l) will collapse back over $E(\tau)$ is:

$$\nu_b(l) = \nu_b^0 \exp[-\tau ba(l-x^*)/kT]. \qquad (6)$$

On the other hand, the probability per unit time for one of the kinks to move forward past the dragging point is

$$\nu_f = \nu_f^0 \exp\{-E_d/kT\}, \qquad (7)$$

if E_d is the activation energy involved in this process. No analysis of the pre-exponentials ν_f^0 and ν_b^0 is presented here, but we shall assume for simplicity

[15] F. Kroupa and L. M. Brown, Phil. Mag. 6, 1267 (1961).

$\nu_f{}^0 = \nu_b{}^0$. We limit ourselves to the simple case in which every new kink which has passed one dragging point continues to drift to the end of the line. This will be the case if the dragging point offers the same barrier to the kink attempting to come back and if the average thermal energy of the kink, $1/2kT$, is smaller than the average energy, $\tau ab\bar{l}$, gained by a kink drifting from one dragging point to the next ($\bar{l}$ is the average separation between dragging points).

With these restrictions, the over-all rate of nucleation on the segment l is

$$\nu(l) = \nu^* \nu_f / (\nu_f + \nu_b). \qquad (8)$$

If $E_d \gg kT$, $\nu(l)$ has the behavior of a step function, differing appreciably from zero only if the length of the segment, l, is larger than $x^* + (E_d/\tau ba)$. The total rate of nucleation on the dislocation line will then depend on the distribution of segment lengths. If the dragging points are distributed at random, the number of segments having length between l and $l+dl$ is $\bar{l}^{-2} \exp(-l/\bar{l})dl$ per unit length of the dislocation line.[16] This distribution function is also used in the Granato-Lücke theory of internal friction.[17] The creation rate of double kinks per unit length of dislocation is now

$$\bar{\nu}(\tau,T) = \int_{x^*}^{\infty} \bar{l}^{-2} \exp\left(-\frac{l}{\bar{l}}\right)\nu(l)dl. \qquad (9)$$

If $\tau ba\bar{l} > \pi kT$, $\nu(l)$ can be replaced by a step function, and the result of integration is (see Appendix C)

$$\bar{\nu}(\tau,T) = \left(1 + \frac{E_d}{\tau ab\bar{l}} + \frac{x^*}{\bar{l}}\right)\frac{\nu_0{}^*}{a}$$

$$\times \exp\left(-\frac{E(\tau)}{kT} - \frac{E_d}{\tau ab\bar{l}} - \frac{x^*}{\bar{l}}\right). \qquad (10a)$$

In Appendixes A and B, the frequency $\nu_0{}^*$ has been worked out for two simple cases of the force law. For Fig. 1(a), Eq. (B20)

$$\nu_0{}^* = \frac{4c_s E_p}{\pi^2 a E_0}\left(\frac{2\pi E(\tau)}{kT}\right)^{1/2}\{\Pi_3\}. \qquad (10b)$$

For the extreme broken bond model, Fig. 1(c), Eq. (B22)

$$\nu_0{}^* = \frac{ac_s E_p}{2\pi^2 E_0 a_1{}^2}\left(\frac{2\pi E(\tau)}{kT}\right)^{1/2}\{\Pi_3\}, \qquad (10c)$$

E_p is the Peierls energy, E_0 the strain energy of the dislocation, and c_s the velocity of shear sound in the medium. Π_3 is a function defined in Appendix B, which is numerically of the order of 1–10 for germanium. Both $E(\tau)$ and Π_3 are functions of stress. In the pre-

exponential, the stress dependence of $E(\tau)$ can safely be ignored; however, in the exponential, the stress dependence is important and will be approximated by Eq. (2). In germanium, the function, Π_Q, varies with stress and this variation is discussed in Appendix B (Fig. 9) and Sec. IV.

Finally, the dislocation velocity is given by the combination of Eq. (10) with

$$v = 2\bar{\nu}a\lambda, \qquad (11)$$

where λ is the appropriate mean free paths of kinks. There are two cases:

(1) If every kink moves to the end of the line without annihilating with a kink of the opposite sign, λ will equal half the line length L, so that

$$v = \bar{\nu}aL. \qquad (12)$$

(2) In the case where λ is limited by kink collisions, a simple argument[18] gives

$$v = a(2\bar{\nu}\nu_f \bar{l})^{1/2}. \qquad (13)$$

In Appendix D, Eq. (13) is shown to be valid in the case of collisions by uniformly distributed kinks. The rate limiting process is the one giving the shorter λ, or the smaller v.

In either of the above cases, the theory will give essentially the same form of stress and temperature dependence, though with different parameters. At low stress, a term $e^{-\tau_0/\tau}$ will dominate; whereas at high stress, the stress dependence of the activation energy will become important.

IV. COMPARISON WITH EXPERIMENTS ON GERMANIUM

In this section we shall show that there exists a physically reasonable set of parameters with which theory fits closely the experiments of the previous paper, I. The data are, for convenience, replotted in Fig. 4 and Fig. 5 in the form $\ln v$ vs τ^{-1}.

A. 60° Dislocations

Assuming noncolliding kinks, Eq. (12) has been fitted to the data using Eqs. (10) and (2) for $\bar{\nu}$ and $E(\tau)$. The solid curves of Fig. 4 are the result, along with the following values for the various parameters:

$$L\nu_0{}^* = 3\times10^6 \text{ cm/sec}, \qquad (14a)$$

$$E^* = 1.62 \text{ eV}, \qquad (14b)$$

$$x^*/b = 5, \qquad (14c)$$

$$\frac{E_d}{ab\bar{l}} = 0.16 \exp\left[\frac{0.18}{kT(\text{eV})}\right] \text{ kg/mm}^2. \qquad (14d)$$

---

[16] J. S. Koehler, *Imperfections in Nearly Perfect Crystals* (John Wiley & Sons, Inc., New York, 1952), p. 197

[17] A. Granato and K. Lücke, J. Appl. Phys. **27**, 583 (1956).

[18] The drift velocity of nucleated kinks along the line is of the order $\nu_f \bar{l}$. The collision time is then $\lambda/\nu_f \bar{l}$. This must be equal to the time required to nucleate a new double kink, i.e., $(2\bar{\nu}\lambda)^{-1}$. Solving for λ we get (13) from (11). This result was also given by Lothe and Hirth (reference 14).
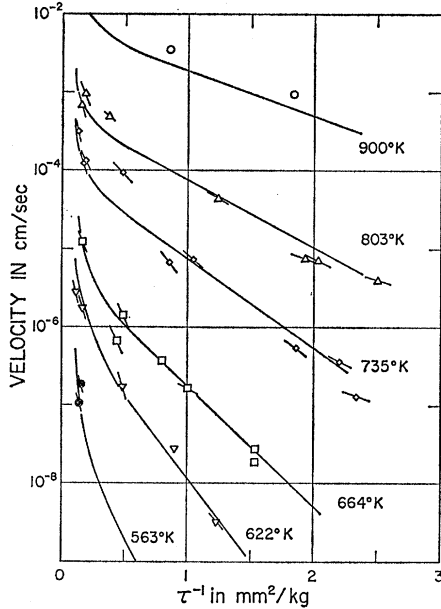
FIG. 4. Velocity of 60° dislocations in Ge as a function of stress, τ. For comparison with theory, $\ln v$ is plotted against $1/\tau$.

It is reasonable to ascribe the temperature dependence of Eq. (14d), to the dragging point spacing $\bar{l}$; that is,

$$\bar{l} = \bar{l}_0 e^{-U/kT}. \tag{15}$$

Equation (14d) gives only the ratio $E_d/\bar{l}$. To determine the range of possible values of $\bar{l}$ and E_d, we accept the following restrictions:

(1) The approximation made in evaluating Eq. (9) is valid, that is, $\tau ab\bar{l} > \pi kT$,

(2) Within the experimental range of temperature and stress, kink collisions do not occur. If collisions began within this range, a fairly abrupt break in the curves should be apparent, which is not the case. This condition may be expressed by

$$\frac{L}{2} < \frac{a\bar{l}\nu_f}{v} = \frac{a\bar{l}\nu_f{}^0}{v} e^{-E_d/kT} \tag{16}$$

which gives, in conjunction with Eq. (14d), an upper (temperature-dependent) limit on $\bar{l}$.

If we choose physically acceptable values for L and $\nu_0{}^*$ [consistent with Eq. (14a)] and make the order of magnitude assumption that $\nu_f{}^0 = \nu_0{}^*$, then the above two conditions establish the range of $\bar{l}$ and E_d within which the noncollision theory is valid. The first two columns of Table I show this range for two choices of L, the consideration being that L should be substantially greater than $\bar{l}$ but no larger than the experimental sizes of the dislocation loops, several tens of microns.

If, on the other hand, the data are assumed to lie within the range where kink collisions dominate, then Eq. (13) must be applied. The curves obtained are, of

TABLE I. Numerical values of parameters for 60° dislocations.

	No collision	No collision	Collision
E^*	1.62 eV	1.62 eV	1.82 eV
E_d	$0.4 < E_d < 0.9$ eV	$0.4 < E_d < 0.55$	0.76 eV
U	0.18 eV	0.18 eV	0.22 eV
$\nu_0{}^* = \nu_f{}^0$	10^{11}/sec	10^{10}/sec	0.6×10^{11}/sec
x^*/b	5	5	11
L	0.3μ	3μ	>1 cm
$\bar{l}_0/b$	$1.8 \times 10^3 E_d$ (in eV)	$1.8 \times 10^3 E_d$ (in eV)	1.42×10^3
$\bar{l}/b$ at 664°K	$70 E_d$ (in eV)	$70 E_d$ (in eV)	28

course, nearly identical to those shown for Eq. (12). However, there does not exist a physically reasonable set of parameters which satisfies the restrictions imposed in the noncollision case above. [Using Eq. (16) in the collision case, the inequality sign is reversed.] We have chosen to display this situation [column three of Table I] by picking the extreme allowed values of the parameters with the object of minimizing L. The result is $L > 1$ cm, which is much larger than the dislocation loop dimensions. One concludes that the experiments are better represented by the noncollision model, Eq. (12).

B. Screw Dislocations

The data for screw dislocations does not present the clear picture developed for the 60° case. As discussed in the previous paper, I, the screw velocity measurements were subject to experimental difficulties from surface cooling. Therefore, they should be considered somewhat less accurate at low stress than the 60° data.
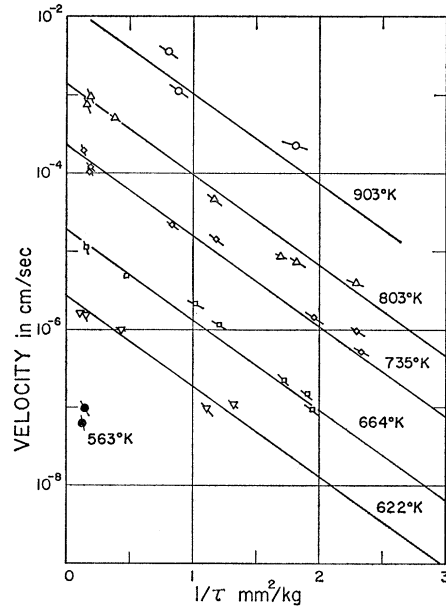

FIG. 5. Velocity of screw dislocations in Ge as a function of stress, τ. Here $\ln v$ is plotted as a function of $1/\tau$.

TABLE II. Numerical values of parameters for screw dislocations

	No collision	No collision	No collision
E^*	1.47 eV	1.47 eV	2.07 eV
E_d	$0.44 < E_d < 0.9$	$0.44 < E_d < 0.55$	0.87 eV
U	~ 0	~ 0	~ 0
$\nu_0^* = \nu_J{}^0$	10^{11}/sec	10^{10}/sec	1.1×10^{13}/sec
x^*/b	...	...	...
L	0.4μ	4μ	>0.6 cm
l/b	$1.1 \times 10^2 E_d$	$1.1 \times 10^2 E_d$	48

We have fitted the screw data in the same manner as the 60°; ignoring, however, the increasing slope of the high stress points in Fig. 5. This procedure misrepresents the most accurate data, where the stress dependence of $E(\tau)$ becomes important. Nevertheless, the similarity between the high stress screw and 60° results indicates that approximately the same $E(\tau)$ will apply to both types of dislocation; that is, the x^* values are comparable.

The parameters derived from this simplified fitting procedure for screws are given in Table II. The validity criteria were the same as those for the 60° cases. We are again led to the conclusion that kink collisions are not dominant, but the over-all situation is not as clear as it was for 60° dislocations.

We note that the slopes of the curves of Fig. 5 are the same, implying that the dragging point spacing, l for screws is independent of temperature.

One interesting apparent tendency for the screws is the lower slopes in Fig. 5 observed in the intermediate stress region. This flattening in the middle of the screw curves, although not completely resolved above the experimental uncertainty, is discussed in a later paragraph of this section.

C. Quantitative Comparison of Parameters

Of the various parameters determined above, ν_0^*, E^*, and x^* are intrinsic properties of the dislocations and one can compare these values with *a priori* estimates. All the other parameters cannot be discussed without knowledge of the nature of the dragging points.

Appendix B gives two different formulas for ν_0^*, (B20) or (B22), depending on whether the potential function of the dislocation is like Fig. 1(a) or Fig. 1(c), respectively. Numerically, the parameters to be used in these formulas are

$$E_0 = 10.3 \times 10^7 \text{ eV/cm},$$
$$E_p = 0.26 \times 10^7 \text{ eV/cm},$$
$$c_s = 4.62 \times 10^5 \text{ cm/sec},$$
$$a = 3.42 \text{ Å},$$

where E_p is the Peierls energy, and E_0 is estimated as the self-energy of that part of the dislocation strain field which is within one wavelength of the vibrating core. (This is the effective mass effect for an accelerating

dislocation discussed by Eshelby.[19]) E_p is given by Celli.[10] In the first case Fig. 1(a), Eqs. (B19) and (B20) then give $\nu_0^* \simeq 2 \times 10^{13}$ at 700°K when $P = 16 E_p/a^2$. A stress dependence of ν_0^* occurs in Π_3 and $E(\tau)$. Both these stress dependences are small and can be neglected, especially as $E(\tau)$ appears under a square root. The numerical value of 10^{13} for ν_0^* is rather high when compared with Tables I and II.

In the second case considered in Appendix B [Eq. (B22)], Fig. 1(c), with $P = 2E_p/a_1^2$, the numerical value of ν_0^* at zero stress and with the same parameters as shown is approximately 10^{12}/sec, partly because the magnitude of Π_Q is less. According to Fig. 9, at low stress, $\ln \Pi_Q \simeq 1$. we have taken $a_1 = a/4$ (see Fig. 9). In addition, depending upon the value of a_1 in Fig. 1(c), there is a non-negligible variation of ν_0^* with stress due to the stress dependence of Π_Q. This stress dependence is sketched in Fig. 9 for the case $a_1 = a/4$. When $a_1 = a/2$, there is a negligible stress variation, since Π_Q is a constant. When $a_1 = a/4$, however, Π_Q has a peak at τ' and differs significantly at $\tau = 0$ from its value at the Peierls stress, τ_p. Thus, plotted against $1/\tau$, the logarithms of the velocity should show a hump at $\tau = \tau'$. This is the kind of behavior a close reading of the screw data gives. We do not know, without further more careful measurements of the screw dislocation velocities, whether we are actually observing the variation in Π_Q here described.

On the basis of this discussion, the 60° dislocations fit best the force law of Fig. 1(b) where $a_1 = a/2$ because of the "normal" stress dependence in Fig. 4, while the screws seem to behave more like Fig. 1(c), where $a_1 = a/4$. This assignment may be reasonable on the basis that the screw motion involves snapping bonds and remaking them, whereas when the 60° dislocation moves, a broken bond will always be present.

The theoretical value of ν_0^* seems to disagree by an order of magnitude from that listed in Tables I and II, and this is probably the best agreement one can reasonably expect. The authors would hesitate to push the flexible string model of the kink nucleation too far towards obtaining actual numerical agreement.

Next, E^* and x^* will be evaluated in the case of the potential given in Fig. 1(b). From (A11), one obtains

$$E^* = \frac{a^2 (PE_0)^{1/2}}{2} \tag{17}$$

and

$$x^* = \left(1 - \ln\frac{\tau}{\tau_p}\right)\left(\frac{E_0}{P}\right)^{1/2}. \tag{18}$$

Thus, x^* is slightly dependent on τ. By using the above value of E_0 and with $P = 8E_p/a^2$, one obtains

$$E^* = 0.79 \text{ eV}$$

and

$$x^*/b = 6.4$$

[19] J. Eshelby, Phys. Rev. **90**, 248 (1953).

at $\tau = 10$ kg/mm^2. The disagreement of these values with those shown in Tables I and II implies that E_0 and E_p are a little larger than the above values.

The values of x^* and E^* are computed on the brittle bond model. If the potential law of Fig. 1(a) is used instead, then E^* becomes 1.0 eV with $a_1 = a/4$ which is a better fit to the experimental value. However, on this model, ν_0^* becomes $\simeq 10^{13}$ which is a strong disagreement with the experimental data. We have, therefore, preferred the brittle bond case.

D. The Dragging Points

A satisfactory discussion of the energies E_d and U and the temperature dependence of l cannot be given without more information as to the nature of the dragging points. The following comments are the best that can be done with the available data and differ in significant respects from previous consideration by van Bueren.[20]

As previously stated, for the theory to be valid the dragging points must maintain a constant l and a random distribution along the line for all motion at a given temperature. Obvious candidates which can satisfy this criterion are jogs on the dislocation line, lattice vacancies and/or interstitials and impurities. Though none of these can be positively eliminated, it is hard to see how the concentration of jogs or lattice point defects on the line could decrease with increasing temperature as demanded by Eq. (15). Having been grown in a hydrogen atmosphere, the experimental crystal probably contained a non-negligible amount of this impurity, and it may also have contained up to about 10^{-6} fraction of oxygen.

If impurities are assumed to be responsible, then it must be shown how *moving* dislocations can have the number of impurities given by Eq. (15). Suppose, for simplicity, impurity atoms occupy interstitial sites. There are three ways in which a kink passes through an impurity atom. First is kink motion following release of pinning due to thermal motion of the impurity off the dislocation line. Second is a process in which the impurity keeps its position relative to its neighbors and the dislocation escapes from the impurity. Last is that the impurity makes a simultaneous jump with the kink motion and remains on the dislocation. Then, the time rate of change of the density of trapped impurities contains a term corresponding to the above processes, $-n_k(\nu_f' + \nu_f'')$. We will write ν_f', ν_f'', and ν_f''' as the frequencies for the above three processes, respectively. In addition, the dislocation, due to the motion of kinks, captures new impurities at the rate $l n_1 n_k \nu_f$, where

$$\nu_f = \nu_f' + \nu_f'' + \nu_f''',$$

n_k is the number of kinks per unit length of dislocation and n_1 is the number of impurities in the neighboring

[20] H. G. van Bueren, Physica **26**, 997 (1960).

Peierls valley. Finally, the diffusion of impurities to the dislocation must be added. In steady state, by equating the impurity rate change on the dislocation to zero, one obtains the number of the trapped impurities. Results show that there are two cases which give an impurity density independent of the dislocation velocity. One is the case in which the velocity is slow enough for the impurities to remain in thermal equilibrium with a dislocation. This case is realized for the observed velocities if all values of activation energy for the various processes of impurity motion are smaller than 1 eV. The other is the opposite extreme case, that is, the thermal motion of the impurities can be neglected as compared with the dislocation motion. In this case, the number of the trapped impurities n_i is given by

$$n_i \approx (\nu_f / \nu_f'') \alpha N a, \tag{19}$$

where α is the cross-section diameter of the dislocation and N is the number of dispersed impurities per unit volume. If $\nu_f'' > \nu_f'''$, n_i is independent of temperature (assuming N is independent of temperature). On the other hand, if $\nu_f'' < \nu_f'''$, Eq. (19) gives the temperature dependence demanded by Eq. (15) and the activation energy U is given by the ratio ν_f / ν_f''.

Both this case and the case of low dislocation velocity require a rather high density of interstitial impurities, 10^{17} cm^{-3}, which in our case are probably oxygen or hydrogen. Of course, at the present stage, one can not rule out other mechanisms of dragging which give the pinning distances required by Eq. (15). Further experiments will be necessary to clarify the nature of the dragging points.

E. Split Dislocation

Art et al.[21] have very recently reported evidence that the screw dislocations of Ge are split. Since the models of this paper are based on a simple unsplit dislocation, the argument must be somewhat generalized to apply in this case. We note first that Art et al. report that the split dislocation nodes appear only after prolonged annealing which is interpreted in terms of dislocation climb. We would like to suggest an alternative, namely, that it is possible that the mobile dislocations (especially screws) are in reality not split, and only become so slowly by an annealing process. The reason is that a split dislocation must manufacture dangling bonds which undoubtedly possesss significant energy. Hence, the rearrangement of the core necessary to begin the split of a whole dislocation must make the unsplit dislocation possess a local minimum of energy with a barrier to be surmounted during the splitting process. If the true equilibrium state is one with split dislocations, the activation energy hill to be surmounted will make the process a slow one depending upon the height of the barrier.

[21] A. Art, E. Aerts, P. Delavignette, and S. Amelinckx (to be published).

If the mobile dislocations are themselves split, then the model of dislocation motion must be rephrased. In this case we would expect that the two partials of the dislocation will generate kinks independently and remain correlated only on the average by the generation of an internal stress acting between the two partials when the distance of separation becomes too far from equilibrium. With this statement, the only place where our work does not apply is the calculation of the kink energy on the basis of Celli's calculation of the Peierls energy Eqs. (17) and (18). Since Celli based his work on an atomic model of a simple unsplit dislocation, this estimate in the case of a split dislocation will be in error.

If the moving dislocations are split, they suggest another mechanism for the dragging points. A construction where the dislocation changes from intrinsic to extrinsic should be difficult for a kink on one of the partials to negotiate, and would satisfy our requirements for a dragging point.

APPENDIX A. THE STRING MODEL FOR DISLOCATION KINKS. STATICS.

1. General

In Appendices A and B, we carry out a number of detailed calculations on the flexible string model of the dislocation kink. This model has previously been studied extensively by Seeger and co-workers, as well as by others.[13] The flexible string model is, of course, a drastic simplification of an actual kink on a dislocation, but the analysis is relatively simple, and capable of making definite predictions. In Appendix A, we derive a number of new results concerning kink statics, and in Appendix B, we apply the theory of absolute reaction rates to kink nucleation.

The equation of equilibrium of the dislocation is obtained by finding the extremes of the energy functional,

$$E[y(x)] = \int_{-\infty}^{\infty} dx[\tfrac{1}{2}E_0 y'^2 + E_p(y) - \tau by], \quad (A1)$$

where $y(x)$ indicates the displacement of the dislocation line at the point x, E_0 is the (core) energy per unit length of the dislocation, $E_p(y)$ is the Peierls potential energy. One obtains

$$E_0 y'' - dE_p(y)/dy + \tau b = 0. \quad (A2)$$

Trivial solutions to (A2) describe a dislocation lying straight in a Peierls valley, the displacement from the bottom of the valley being given by the root y_∞ of

$$dE_p(y)/dy = \tau b. \quad (A3)$$

We look for nontrivial solutions of the double kink type, as depicted in Fig. 2. For $x>0$, integration of (A2) yields

$$y' = -[2E_p(y)/E_0 - 2\tau by/E_0 + 2C_1]^{1/2}. \quad (A4)$$

The constant C_1 is determined by requiring that for $x \rightarrow \infty$, y' vanish and y approach the solution y_∞ of (A3). One finds

$$C_1 = \tau by_\infty/E_0 - E_p(y_\infty)/E_0. \quad (A5)$$

Because of the symmetry $y(x) = y(-x)$, y assumes its maximum value y_m at the origin. Putting $y_m' = 0$ in (A4):

$$E_p(y_m) - E_p(y_\infty) = \tau b(y_m - y_\infty). \quad (A6)$$

Inserting (A4) in (A1) and using (A5) and (A6), the energy of the (unstable) equilibrium configuration called the "double kink" is found to be

$$E(\tau) = -2E_0 \int_{y_\infty}^{y_m} y' dy. \quad (A7)$$

The problem is then reduced to quadratures and to the solution of algebraic equations (A3) and (A6). Since $E_p(y)$ is periodic, there are many solutions to (A6) corresponding to the top of the double kink being in the first, second, $\cdots$, nth Peierls valley.

2. Saddle-Point Energy

For particular forms of $E_p(y)$ it is easy to evaluate $E(\tau)$ explicitly. For the case of the profile of Fig. 1(a), made up of pieces of parabolas:

I $\quad E_p(y) = \tfrac{1}{2}Py^2, \quad |y| < a$

II $\quad E_p(y) = \tfrac{1}{4}Paa_1 - Pa_1(a - 2a_1)^{-1}(y - a/2)^2,$
$$\qquad\qquad\qquad\qquad a_1 < y < (a - a_1) \quad (A8)$$

III $\quad E_p(y) = \tfrac{1}{2}P(y - a)^2, \quad |y - a| < a_1.$

In this case in order for (A3) to have a solution, τ must be smaller than Pa_1/b, the Peierls stress. That is, the applied stress must be less than the Peierls stress—a general requirement. To display the result we define the quantities $\sigma = \tau b/Pa_1 < 1$ and $\beta = a/2a_1 \geq 1$. There are two cases:

(a) For $4\beta\sigma \geq (1+\sigma)^2$ (large stresses) the tip of the double kink lies in II of Fig. 1(a) and the energy is

$$E(\tau) = E'(1-\sigma)^2\{1 + (\beta-1)^{1/2}(\pi/2 + s)\},$$
$$s = \sin^{-1}[(1-\beta^{-1})^{1/2}], \quad E' = \tfrac{1}{2}aa_1(PE_0)^{1/2}. \quad (A9a)$$

(b) For $4\beta\sigma \leq (1+\sigma)^2$ (small stresses) the tip of the double kink lies in III of Fig. 1(a) and the energy is

$$E(\tau) = E'\{(1+\sigma)R + (1-\sigma)^2[1 + (\beta-1)^{1/2}(s+s')]$$
$$\qquad\qquad + 2\sigma \ln[(\sigma+1+R)^2/4\beta\sigma]\}, \quad (A9b)$$
$$R = [(1+\sigma)^2 - 4\beta\sigma]^{1/2},$$
$$s' = \sin^{-1}[(1-\beta^{-1})^{1/2}(1+\sigma)(1-\sigma)^{-1}].$$

The energy of two kinks at infinite separation, corresponding to zero-applied stress, is
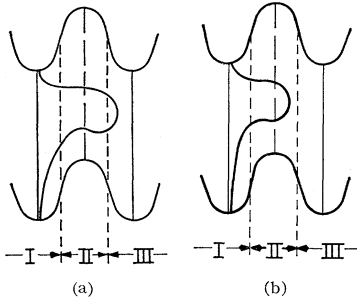
$$E^* = 2E'[1 + s(\beta-1)^{1/2}].$$

FIG. 6. Unstable equilibrium or saddle-point configuration of a kink pair under an external stress. (a) At low stresses the forward nose of the kink reaches well down into the next Peierls trough, region III. (b) At high stresses, the nose remains on the top parabola in region II.

In the case of the profile of Fig. 1(b), $E_p(y)$ is given by

$$E_p(y) = \tfrac{1}{2}Py^2, \qquad |y| < \frac{a}{2}$$

$$E_p(y) = \tfrac{1}{2}P(y-a)^2, \quad |y-a| < \frac{a}{2} .$$

(A10)

For $E(\tau)$ we obtain

$$E(\tau) = E^*\left[1 - \frac{\tau}{\tau_p} + \frac{\tau}{\tau_p}\ln(\tau/\tau_p)\right], \qquad (A11)$$

where $\tau_p = Pa/2b$ is, in this case, the Peierls stress and $E^* = (a^2/2)(E_0P)^{1/2}$ is again the energy of the two kinks at infinite separation. In this case, in order for (A3) to have a solution, $\tau b < Pa/2$, that is the applied stress must be smaller than the Peierls stress.

Finally, consider a Peierls energy profile of the type drawn in Fig. 1(c).

I $E_p(y) = \tfrac{1}{2}Py^2,$ $|y| < a$

II $E_p(y) = \tfrac{1}{2}Pa_1^2,$ $a_1 < y < (a-a_1)$ (A12a)

III $E_p(y) = \tfrac{1}{2}P(y-a)^2,$ $|y-a| < a_1.$

When the tip of the double kink lies on the plateau (region II) we get

$$E(\tau) = (PE_0/3)(a_1 - \tau a/P)^2(1 + 2Pa_1/\tau b). \quad (A12b)$$

In this case a τ^{-1} dependence on stress is obtained. This is not surprising because the model is the same as was used by Fisher[22] to describe a dislocation trying to break away from a uniform distribution of pinning points. Gilman[23] has used this model to explain the LiF data, despite the objection that it is not clear why the dislocation should stop again after the breakaway. If we suppose that the dislocation is caught in another similar groove at a distance a from the first, that is, it enters into region III of Fig. 1(c), then it can be shown (except when τ is very close to the Peierls stress), that the τ^{-1} term disappears and the τ dependence is almost linear, as in the case of the parabolic Peierls potentials.

[22] J. C. Fisher, Trans. Am. Soc. Metals **47**, 451 (1955).
[23] J. J. Gilman, Australian J. Phys. **13**, 326 (1960).

3. Kink Widths

We have need in Appendix B for the width of a kink as a function of the external stress [actually the width of the kink lying in region II of Fig. 1(a)].

For the case of Fig. 1(a), Eq. (A2) is the pertinent equation, where the restoring force, $-dE_p/dy$, called henceforth $f(y)$, is given by

$$f(y) = -\frac{dE_p}{dy} = -P\begin{cases} y & \text{I} & |y| < a/4 \\ -(y-a/2) & \text{II} & a/4 < y < 3a/4 \\ y-a & \text{III} & \dfrac{3a}{4} < y \end{cases}$$

$$P = 16E_p/a^2; \quad a_1 = a/4. \tag{A13}$$

As pointed out in the last section, there is one type of solution for low stresses less than a critical stress τ', and a second type for stresses higher than τ', where τ' is given by

$$\tau' = \frac{Pa}{4b}\cdot\frac{\sqrt{2}-1}{\sqrt{2}+1}. \tag{A14}$$

For low stresses the tip of the kink reaches into region III of Fig. 1(a). With (A13), Eq. (A2) then becomes a double "well" problem for low stresses and standard analysis of the well problem using the usual boundary conditions that $y(x)$ and $y'(x)$ are continuous at the well corners yields the following condition for the length of line lying in region II, $\tau < \tau'$

$$\cos\left(\frac{1}{2}\gamma X_{\text{II}} + \frac{\pi}{4}\right) = \frac{\tau b/P + a/4}{2(\tau b/P - a/4)}, \quad \gamma^2 = P/E_0. \quad (A15)$$

Here, X_{II} is the total width of the segments of the dislocation lying in region II.

For high stresses, $\tau > \tau'$, the low stress solution breaks down and the forward tip of the kink does not reach into region III. Thus, the solution appropriate for high stress is depicted in Fig. 6(b), and analysis as before yields

$$X_{\text{II}} = \frac{3\pi}{2}\left(\frac{E_0}{P}\right)^{1/2} = \frac{3\pi a}{8}\left(\frac{E_0}{E_p}\right)^{1/2}, \quad Pa/4b > \tau > \tau'. \quad (A16)$$

In the high stress case, X_{II} is not a function of the stress. However, of course τ is limited below the Peierls stress, $Pa/4b$.

A rough sketch of X_{II} as a function of stress is given in Fig. 7 for the case of Fig. 1(a).

For the brittle bond case of Fig. 1(c), the lines of the argument are the same as before. The force law is given in Eq. (A12). There are again two stress regimes. At low stress, the nose of the double kink reaches into region III, while at high stress, the nose reaches only
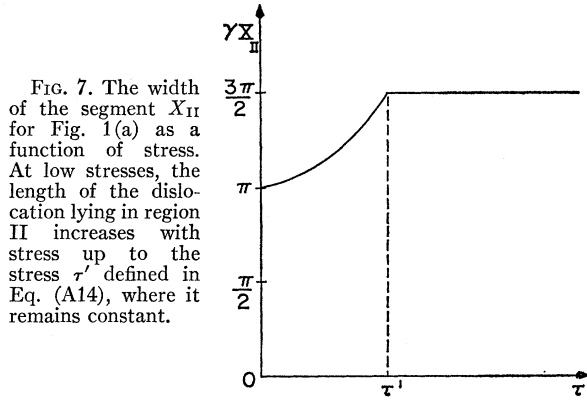
FIG. 7. The width of the segment X_{II} for Fig. 1(a) as a function of stress. At low stresses, the length of the dislocation lying in region II increases with stress up to the stress τ' defined in Eq. (A14), where it remains constant.

to region II. The parameter X_{II} has been calculated for low and high stresses.

$$\tau'/\tau_p=\left(\frac{a}{a_1}-1\right)-\left[\frac{a}{a_1}\left(\frac{a}{a_1}-2\right)\right]^{1/2}.$$

For $\tau>\tau'$,

$$X_{II}=\frac{2}{\tau b}(PE_0)^{1/2}\left(a_1-\frac{\tau b}{P}\right). \tag{A17}$$

For $\tau<\tau'$

$$X_{II}=\frac{2a_1}{b}(PE_0)^{1/2}\left\{\left(\frac{1}{\tau}-\frac{1}{\tau_p}\right)-\left[\left(\frac{1}{\tau}+\frac{1}{\tau_p}\right)^2-\frac{2a}{\tau\tau_pa_1}\right]^{1/2}\right\}.$$

a_1 is the parameter shown in Fig. 1(c) and defined in (A11). In this case, the Peierls stress, τ_p, is given by

$$\tau_p=2E_p/a_1b. \tag{A18}$$

APPENDIX B. THE STRING MODEL FOR DISLOCATION KINKS. KINK NUCLEATION RATE[24]

1. Vineyard's Formula

Vineyard[25] has given the following formula for the transition rate between two stable configurations which are separated by a single saddle point

$$\nu^*=\left(\frac{kT}{2\pi}\right)^{1/2}\int_S e^{-\varphi/kT}dS \bigg/ \int_A e^{-\varphi/kT}dy. \tag{B1}$$

(What Vineyard has termed Γ is here called ν^*.) The surface S is a hypersurface drawn through the saddle point dividing the region of configuration space around the first stable configuration (A) from that of the second. φ is the configuration potential function. The integral over A is an integral over the volume in configuration space near the first configuration, I. In

this formula, configuration coordinates are chosen to contain the masses of the system, so that the kinetic energy is written as a sum over the modes as $\sum_i \frac{1}{2}\dot{y}_i^2$, and the potential energy is likewise written $\sum_i 2\pi^2\nu_i^2 y_i^2$.

When the potential energy at A and at the saddle point within the hypersurface can be represented as a set of oscillators, then Vineyard's formula takes on the simple form

$$\nu^*=\nu_0^* e^{-E^*/kT},$$

where

$$\nu_0^*=\prod_j \nu_j/\prod_j \nu_j', \tag{B1-a}$$

where E^* is the activation energy, and ν_j and ν_j' are the frequencies in the ground state and activated state, respectively. We find reason to modify this latter form of the equation, however.

We make the basic assumption, which has never been wholly justified, that the modes of the entire crystal can be separated into two noninteracting classes—dislocation modes and crystal modes. The dislocation modes M are assumed to be given by the vibrating string model with Peierls troughs. In order to apply the Vineyard formula, we need only find the dislocation modes in the activated state and compare them with those in the stable configuration.

2. Stable Configuration

In the stable configuration, called I, with the dislocation lying in a single Peierls trough, the equation of motion of the string in the presence of an external stress, τ, is

$$\frac{\partial^2 y}{\partial x^2}-\frac{P}{E_0}y+\frac{\tau b}{E_0}=\frac{1}{c_s^2}\ddot{y}. \tag{B2}$$

The quantities in this equation are the same as in Appendix A, except that $c_s^2=E_0/M$, where M is the inertial mass density of the dislocation core, and E_0 is the rest energy density of the dislocation core. The "sound velocity" along the dislocation thus defined depends somewhat on the frequency as shown by Eshelby,[19] but we shall simply take it to be the shear sound velocity of the medium. The running wave solutions of this equation yield a dispersion relation given by

$$y_j=\exp[i(k_jx-2\pi\nu_jt)]+\tau b/P,$$
$$k_j=2\pi j/l, \quad j=(1,\cdots,N), \tag{B3}$$
$$4\pi^2\nu_j^2/c_s^2=P/E_0+k_j^2.$$

An important point is that the frequency does not approach zero as k goes to zero, but rather $2\pi\nu\to Pc_s^2/E_0$. l is the length of line between two pinning points, N is the number of atoms in this length.

3. Saddle Configuration

We now solve the dynamic equation of motion, (B2), for small oscillations about the static equilibrium saddle point given in Appendix A, and employ the

---

[24] The type of analysis carried out in this Appendix was first applied to pinned dislocations by L. J. Teutonico, A. V. Granato, and K. Lücke, Bull. Am. Phys. Soc. 7, 223 (1962), and these authors have independently worked out a similar problem to ours in a different connection in a forthcoming paper.
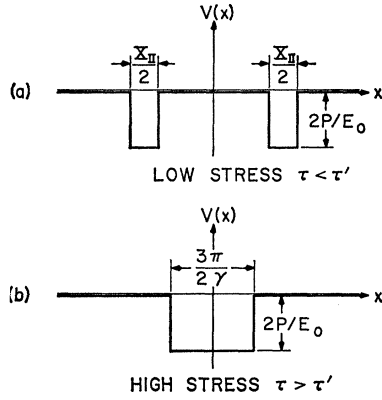
[25] G. Vineyard, J. Phys. Chem. Solids 3, 121 (1957).

FIG. 8. Plot of $V(x)$ of Eq. (B8). (a) For low stress, $\tau < \tau'$ [see Eq. (A14)], the function is a double well of depth $2\gamma^2$, with $\gamma^2 = P/E$. The width of each segment of the well is $\frac{1}{2}X_{\mathrm{II}}$, where X_{II} varies with stresses in the manner shown in Fig. 7. (b) For high stress, $\tau > \tau'$ the double well combines into a single well of depth $2\gamma^2$ and constant width, $X_{\mathrm{II}} = 3\pi/2\gamma$.

method of Hobart,[26] who has analyzed the excitations of a single kink. Let

$$y = y_0 + \xi e^{i2\pi\nu t}, \qquad (B4)$$

where y_0 is the static solution given by (A2), rewritten

$$\frac{\partial^2 y_0}{\partial x^2} + \frac{1}{E_0} f(y_0) + \frac{\tau b}{E_0} = 0. \qquad (B5)$$

Expanding f,

$$f(y) = f(y_0) + \xi \frac{df(y_0)}{dy_0}, \qquad (B6)$$

then

$$\frac{d^2\xi}{dx^2} + \left(\frac{1}{E_0} \frac{df(y_0)}{dy_0} + \frac{4\pi^2\nu^2}{c_s^2} \right)\xi = 0 \qquad (B7)$$

to first order, assuming that $\tau b^2 \ll E_p$. The term, $df(y_0)/dy_0$ is a known function of x, once the static saddle-point configuration is known.

We again adopt the simple law of force with equal pieced upper and lower parabolas where $a_1 = a/4$ in Fig. 1(a). This is the force law given in Appendix, Sec. A3, and Eq. (A8). The low-stress and high-stress solutions are depicted in Figs. 4(a) and 4(b), and discussed in the Appendix, Sec. A3.

The small vibration equation (B7), becomes a simple one-dimensional "well" problem for high stress, and a double-well problem for low stress, equivalent to the simple Schrödinger equation in one dimension for well-type potential functions. We make use of this analogy to write (B7) in the form

$$d^2\xi/dx^2 + [\lambda - V(x)]\xi = 0, \quad \lambda = 4\pi^2\nu^2/c_s^2 - P/E_0, \quad (B8)$$

λ is the eigenvalue. Then V has the form sketched in Fig. 8 with the depth $2P/E_0$. If λ is positive, the solutions are running waves with local perturbations in the region of the kink. These solutions correspond to the scattering of a free particle in the quantum analog. If λ is negative, corresponding to a bound state in the quantum analog, the solution is a localized

[26] R. Hobart, thesis, University of Illinois, 1961 (unpublished).

vibration which is damped out in regions away from the kink. If $\lambda < -P/E_0$, the solution possesses an imaginary frequency and is an unstable oscillation, corresponding to the kink expanding into the next Peierls trough. We shall analyze these three types of solutions separately.

4. Running Wave Solutions

For the running waves, the quantity of interest is the frequency shift compared to the unkinked straight dislocation. This shift corresponds to the energy shift in the quantum analog, and we can obtain the desired result by perturbation theory. The unperturbed equation is Eq. (B2). To first order,

$$\delta\lambda = \delta\left(\frac{4\pi^2\nu^2}{c_s^2}\right) = \frac{1}{l}\int_{-l/2}^{l/2} V(x)dx.$$

Thus,

$$2\pi\delta\nu = -(PX_{\mathrm{II}}/E_0 l)(c_s^2/2\pi\nu), \qquad (B10)$$

l is the length of the segment between pinning points. The quantity, X_{II}, is the total length of line in region II, and is given by (A15) and (A16) for the two cases. This formula for the frequency shift is valid for the higher excitation modes of the kinks where perturbation theory is valid.

5. Localized and Translation Modes

The low-frequency modes, though relatively few in number, are more drastically changed, and perturbation theory cannot be applied. In particular, when λ becomes negative, the vibration is no longer a running wave, but becomes a localized mode. The solution of (B8) for a specific mode for the low- and high-stress cases is $(x > 0)$. Low stress, $\lambda < 0$, $x > 0$.

$$\xi_{\mathrm{I}} = A\exp[-(-\lambda)^{1/2}x], \qquad y < a/4$$

$$\xi_{\mathrm{II}} = B\cos(\kappa x - \beta), \qquad a/4 < y < 3a/4$$

$$\xi_{\mathrm{III}} = C\begin{cases}\cosh(-\lambda)^{1/2}x \\ \sinh(-\lambda)^{1/2}x\end{cases}, \qquad 3a/4 < y \qquad (B11\text{-}a)$$

$$\kappa^2 = 2P/E_0 + \lambda.$$

High stress, $\lambda < 0$, $x > 0$.

$$\xi_{\mathrm{I}} = A\exp[-(-\lambda)^{1/2}x], \qquad y < a/4$$

$$\xi_{\mathrm{II}} = B\begin{cases}\cos\kappa x \\ \sin\kappa x\end{cases}, \qquad a/4 < y < 3a/4 \qquad (B11\text{-}b)$$

$$\kappa^2 = 2P/E_0 + \lambda.$$

The usual boundary conditions are taken. ξ and ξ' are continuous, and for $|x| \to \infty$, $\xi \to 0$. These boundary conditions at the corners of the well are sufficient to fix A, B, β and give the possible localized modes in the usual way.

When λ becomes sufficiently negative, the frequency, ν, becomes imaginary. An imaginary frequency corresponds to the instability of the saddle configuration and is called a "longitudinal translation mode" with a notation which will become clear. From the physical requirement of the saddle configuration, it is, therefore, necessary that there be at least one imaginary frequency, and, indeed, we now show that there is just one.

One could carry out this demonstration by manipulating the functions at the corners of the potential well in the standard manner, and, indeed, the functional conditions giving possible values of κ are simple enough to be written analytically. However, we proceed in a more general manner which is valid for any assumed Peierls force model.

We begin by noting that the solutions (B11) contain both symmetric (cos, cosh) and antisymmetric solutions (sin, sinh). The lowest symmetric solution corresponds to an expanding kink pair in which both members of the kink move in opposite directions, tending to expand or contract the kink pair. The lowest antisymmetric mode has one node at the tip of the kink where $x=0$. In this mode both sides of the kink pair move in the same direction, and their net separation is not changed during the vibration. This lowest antisymmetric mode thus simply corresponds to a translating kink pair, with each kink moving in the same direction while keeping the same separation. We shall call this mode the "transverse translation mode" in an obvious language. A simple transverse translation mode must have $\nu=0$, and such a zero frequency mode exists on the grounds that the whole equation system, (B2), is invariant to rigid translation along the x axis. One can of course, also demonstrate directly, using the solutions (B11) and the boundary conditions as outlined above, that a mode $\nu=0$ does, in fact, exist.

From the general properties of differential equations, one knows that the eigenvalue for the lowest symmetric mode with no nodes lies below the lowest eigenvalue of the antisymmetric mode with one. Hence the result is: (1) There is just one longitudinal translation mode or breathing mode with imaginary frequency; (2) there is one transverse translation mode with zero frequency; and (3) all other modes have real frequencies, although, in general, there may exist localized modes with negative λ.

The existence of the transverse translation mode, however, means that (B1a) cannot be used directly for the nucleation rate. For this particular mode of the dislocation, the phase integral in (B1) becomes simply

$$\int_{-\frac{1}{2}M_k^{\frac{1}{2}}l}^{\frac{1}{2}M_k^{\frac{1}{2}}l} dy = M_k^{\frac{1}{2}}l, \qquad (B12)$$

where M_k is the kink "mass" and l is the length of the segment between pinning points.

The mass of the kink appearing in (B12) is defined in terms of the kinetic energy of the transverse trans-

lation mode,

$$E(\tau,v) = E(\tau,0) + \tfrac{1}{2}M_k v^2, \qquad (B13)$$

where v is the velocity of translation of the kink pair. This mass is obtained by appeal to the relativistic analogy in Eq. (B2). By quite general arguments similar to those of Hobart[26] one can show that

$$E(\tau,0) = M_k c_s^2, \qquad (B14)$$

where c_s is the shear sound velocity of the medium.

With (B12) then, after Vineyard, (B1) becomes

$$\nu^* = l\left(\frac{2\pi M_k}{kT}\right)^{1/2}\left(\prod_{j=1}^{N}\nu_j \Big/ \prod_{j=3}^{N}\nu_j'\right)e^{-E(\tau)/kT},$$
$$\qquad (B15)$$
$$= \frac{l}{a}\nu_0^* e^{-E(\tau)/kT}.$$

In this equation, we deviate from Vineyard's notation in (B1-a). Here, we label the two translation modes as 1 and 2, leaving $N-2$ oscillator modes, ν_j'; $j=3, 4, \cdots, N$.

6. Calculation of Nucleation Rate

Using the perturbation results of (B10), the products of (B15) are easily computed for the high-frequency modes. Introducing a convenient quantity, Π_Q, defined by

$$\Pi_Q = \prod_{j=Q}^{N}\nu_j \Big/ \prod_{j=Q}^{N}\nu_j', \qquad (B16)$$

then

$$\ln\Pi_Q = -\sum_{j=Q}^{N}\ln\frac{\nu_j+\delta\nu_j}{\nu_j}\simeq -\sum_{j=Q}^{N}\frac{\delta\nu_j}{\nu_j}. \qquad (B17)$$

The sums in this equation are taken over only the higher modes where $Q\gg1$, and the perturbation approach is valid. Substitution of (B10) gives

$$\ln\Pi_Q = \sum\frac{PX_{II}}{lE_0}\frac{1}{k^2+P/E_0}$$
$$\simeq \frac{2PX_{II}}{lE_0}\int_0^N\frac{dn}{(2\pi n/l)^2+P/E_0}. \qquad (B18)$$

In this equation, the lower limit in the integral is taken as zero because the cutoff for perturbation theory is below $k=(P/E_0)^{1/2}$, and contributions to the integral from the region near the lower limit are negligible. Finally, using the value of X_{II} given in (A15) and (A16) for the low- and high-stress regimes,

$$\Pi_Q = e^{\pi/2} \to e^{3\pi/4} \quad \text{low stress}$$
$$= e^{3\pi/4} \qquad \text{high stress.} \qquad (B19)$$

The shift in value at low stress is a gradual effect caused by the smooth part of the curve in Fig. 7, while at high stress X_{II} is stress-independent.

Equation (B19) is only valid for $Q \gg 1$; for Q of the order of one, perturbation theory is not valid. For running waves, we do not expect the results of (B19) to be greatly wrong even at low frequency. However, if any localized modes should exist, their frequencies might differ markedly from the corresponding modes in the stable configuration. We have not carried out a detailed treatment of the localized modes of the low-stress regime, although one can show easily enough that no localized modes exist in the high-stress regime, suggesting that at low stresses, never more than one localized mode could exist. Actually, we would expect that the details of the localized mode picture will depend upon the specific model chosen for the Peierls energy, and such results probably would have no significance without more information on actual kink structure. But although detailed results are not available, one can make a number of qualitative statements about the product quotient in (B15) for the low frequencies.

In particular, the *stress dependence* of the product quotient can be determined. We note that at the transition between two wells and the single well, the width of the total length of well remains constant, and that the depth of the well also remains fixed. Hence, the eigenvalue, λ, and ν' must remain unchanged to first order.

If we neglect the considerations of the past two paragraphs, and write the product quotient in (B15) entirely in the perturbation theory, we have in that approximation.

$$\nu^*(l,\tau) = -\nu_0^*(\tau)e^{-E(\tau)/kT},$$

$$\nu_0^*(\tau) = \frac{ac_sP}{4\pi^2 E_0}\left[\frac{2\pi E(\tau)}{kT}\right]^{1/2}\{\Pi_3\}. \qquad (B20)$$

Π_3 is the function in (B19) with $Q=3$. It must be remembered that this formula is computed for the case of equal upper and lower parabolas. For this case, P is given by $P = 16E_p/a^2$.

7. Brittle Bond Model

The previous sections of this Appendix have explicitly assumed the model of matched equal parabolas in the force law of Fig. 1(a). However, in the diamond lattice, it is more reasonable to adopt a force law which reflects the intuitive picture of chemical bonds between atoms which have only a limited flexibility. Thus, in a simple unsplit screw dislocation, the bonds between the atoms of the core must be snapped off and reconnected as the dislocation moves. (In the 60° dislocation, or a split screw dislocation the existence of dangling bonds makes the motion possibly more smooth.) Thus, calculations are here reproduced for a force law of type Fig. 1(c).

The analysis of the saddle-point configuration proceeds as before and (B20) is again valid. In this case, $P = 2E_p/a_1^2$. The function Π_Q is, of course, different because of the different function $V(x)$ in (B8) and because X_{II} is a different function. The form of $V(x)$ is the same as before, but the depth is only P/E_0. The results are:

high stress, $\tau > \tau'$,

$$\ln\Pi_Q = \frac{1}{2}\left(\frac{\tau_p}{\tau} - 1\right); \qquad (B21)$$

low stress, $\tau < \tau'$,

$$\ln\Pi_Q = \frac{1}{2}\left\{\left(\frac{\tau_p}{\tau} - 1\right) - \left[\left(\frac{\tau_p}{\tau} + 1\right)^2 - \frac{2\tau_p a}{\tau a_1}\right]^{1/2}\right\}$$

which take the place of (B19). ν_0^* is now given by (B21) with (B20), together with the relation $P = 2E_p/a_1^2$:

$$\nu_0^* = \frac{ac_sE_p}{2\pi^2 E_0 a_1^2}\left[\frac{2\pi E(\tau)}{kT}\right]^{1/2}\{\Pi_3\}. \qquad (B22)$$

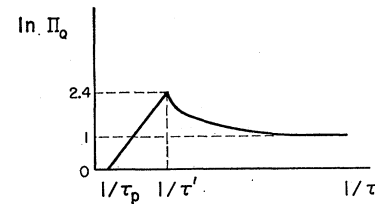This equation is valid, of course, only in the case of Fig. 1(c).

FIG. 9. Schematic dependence of the function Π_Q as function of stress in the brittle bond model for $a_1 = a/4$. $\ln\pi_Q$ goes to one at $\tau = 0$ with a peak at $\tau = \tau'$.

These equations lead to a more interesting stress dependence than (B20) and (B19). Dislocation velocity is discussed in Sec. IV of the main text, but Fig. 9 shows the stress dependence of $\ln\Pi_3$ for $a_1 = a/4$. For the special case $a_1 = a/2$, $\ln\Pi_3 = 0$.

APPENDIX C

From (5) through (9) we obtain:

$$\nu^*(T,\tau) = \frac{\nu_0^*\alpha^2}{b}\exp\left[-\frac{E(\tau)}{kT}\right]\frac{d}{d\alpha}[-Ie^{-\alpha(v+u)}], \qquad (C1)$$

where $u = \tau bax^*/kT$, $v = E_d/kT$, $\alpha = kT/\tau ba\bar{l}$, and the integral I can be reduced to the form:

$$I = \int_0^{e^v}\frac{t^{\alpha-1}}{1+t}dt \qquad (C2)$$

with the substitution $t = \exp\{[E_d - \tau ba(l - x^*)]/kT\}$. When α is smaller than one, I can be divided into two parts, thus:

$$I = I_1 + I_2 = \int_0^\infty - \int_{e^v}^\infty. \qquad (C3)$$

I_1 is given in closed form, $I_1 = \pi/\sin\pi\alpha$, and I_2 can be evaluated by expanding the denominator. The leading term in the resulting series is of order $\exp(-v)$ compared to I_1. If this can be neglected and if $\sin\pi\alpha$ can be replaced by $\pi\alpha$, we obtain formula (10a) for $\bar{\nu}(T,\tau)$. This result is valid if $E_d > \tau ba x^*$ and $\tau ba \bar{l} > \pi kT$.

APPENDIX D

In this Appendix, collisions of kinks are discussed on the basis of the model mentioned in Sec. III. We restrict ourselves to the case of a dislocation of infinite length.

The dragging points on the dislocation are labeled with an index q running from $-\infty$ to ∞. Let $F_l(q,p)$ [and $F_r(q,p)$] be the probability that a left- (right-) side kink, which is produced on the segment between the pinning points q and $q+1$, can reach the pinning point p. Then the number of left-side kinks reaching the pinning point p per unit time is

$$n_l(p) = \sum_{q=p}^{+\infty} \nu_q F_l(q,p),$$

where $\nu_q = \nu(l_q)$ is the over-all rate of nucleation of double kinks on the segment $(q, q+1)$, and is given by (8) as a function of the length l_q of the segment. Each kink remains at the point p for a time ν_f^{-1}, and, therefore, the pinning point p is occupied by left-side kinks for the time $n_l(p)/\nu_f$. The probability $f_r(p)$ that a right-side kink will collide with a left-side kink at the pinning point p is then given by

$$f_r(p) = 2n_l(p)/\nu_f. \tag{D1}$$

The factor 2 comes from the fact that a right-side kink also stays at the point for $1/\nu_f$ sec. The collision probability $f_l(p)$ for left-side kinks is derived in a similar way:

$$f_l(p) = \frac{2}{\nu_f} \sum_{q=-\infty}^{p-1} \nu_q F_r(q,p). \tag{D2}$$

The continuity equation for the current of right-side kinks generated on the segment $(q, q+1)$ leads to:

$$F_r(q,p)f_r(p) = F_r(q,p) - F_r(q, p+1), \tag{D3}$$

for $q > p$; similarly for the left-side kinks:

$$F_l(q,p)f_l(p) = F_l(q,p) - F_l(q, p-1), \tag{D4}$$

for $q > p$. Equations (D1) to (D4) are the fundamental equations for collisions of kinks. From the definition of $F_r(q,p)$ and $F_l(q,p)$,

$$F_r(p, p+1) = F_l(p,p) = 1. \tag{D5}$$

Using the above equations together with (D5) one obtains

$$f_r(p+1) - f_r(p) = f_r(p+1)f_l(p+1) - 2\nu_p/\nu_f \tag{D6}$$

and

$$f_l(p+1) - f_l(p) = -f_r(p)f_l(p) + 2\nu_p/\nu_f. \tag{D7}$$

By adding (D6) and (D7),

$$f_r(p+1) + f_l(p+1) - f_r(p+1)f_l(p+1)$$
$$= f_r(p) + f_l(p) - f_r(p)f_l(p),$$

that is,

$$f_r(p) + f_l(p) - f_r(p)f_l(p) = \text{const} = f. \tag{D8}$$

Inserting (D8) into (D7)

$$f_l(p+1) + f_r(p) = f + 2\nu_p/\nu_f. \tag{D9}$$

As mentioned in Sec. III, only segments longer than $(E_d/\tau ba) + x^*$ produce new kinks. In a region between two neighboring active segments, one easily obtains

$$f_l(p+1) - f_l(p) + f_l(p)f - f_l(p+1)f_l(p) = 0. \tag{D10}$$

This equation can be transformed to

$$\left\{ \frac{1}{f_l(p)} - \frac{1}{f} \right\} \frac{1}{1-f} = \left\{ \frac{1}{f_l(p+1)} - \frac{1}{f} \right\}. \tag{D11}$$

Then, one has a solution for $f_l(p)$:

$$1/f_l(p) - 1/f = c(1-f)^{-p}, \tag{D12}$$

where c is a constant. c has a different value in each nonactive region and solutions in different regions are connected by using Eq. (D9). (D12) is written in a more illuminating way as:

$$f_l(p) = \frac{f}{1 + fc(1-f)^{-p}}, \tag{D13}$$

and from (D8)

$$f_r(p) = \frac{f}{1 + (1/fc)(1-f)^{p+1}}. \tag{D14}$$

f and c are easily determined in the simple case that equally active segments are distributed uniformly. When the distribution function of lengths of segments assumed in Sec. III is used, the distance between adjacent active segments is $\bar{l} \exp(E_d/\tau ba\bar{l} + x^*/\bar{l})$ and the averaged nucleation rate on an active segment is

$$\nu_{av} = \bar{\nu}\bar{l} \exp(E_d/\tau ba\bar{l} + x^*/\bar{l}), \tag{D15}$$

where $\bar{\nu}$ has been given by Eq. (10a).

Suppose that a segment $(0,1)$ is active. Then, a neighboring active one is the segment $(i, i+1)$, where $i = \exp(E_d/\tau ba\bar{l} + x^*/\bar{l})$. Now, the boundary conditions are given as follows:

$$f_l(1) = f_l(i+1), \quad f_l(i+1) + f_r(i) = f + 2\nu_{av}/\nu_f, \tag{D16}$$
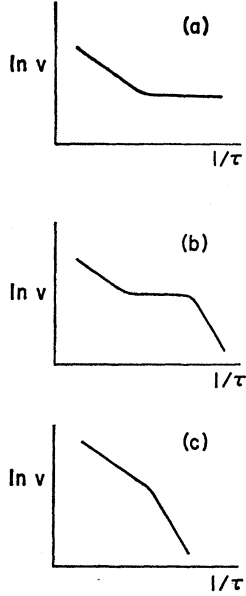
and from symmetry

$$f_l(1) = f_r(i).$$

FIG. 10. Dislocation velocity, v, as a function of applied stress, τ, for dislocations of various lengths, L (schematic drawing). (a) Infinite length; (b) $L > 2l/\alpha$; (c) $L < 2l/\alpha$.

After a little calculation, one obtains

$$f = \frac{1 + (1-f)^{i/2}}{1 - (1-f)^{i/2}} \frac{2\nu_{\mathrm{av}}}{\nu_f} \qquad (D17)$$

and

$$f_c = (1-f)^{i/2+1}.$$

(D17) gives

$$f = \left(\frac{8\nu_{\mathrm{av}}}{i\nu_f}\right)^{1/2} = 2\left(\frac{2\nu_{\mathrm{av}}}{\nu_f}\right)^{1/2} \exp\left(-\frac{E_d}{2\tau ab\bar{l}} - \frac{x^*}{2\bar{l}}\right) \qquad (D18)$$

in the case of $fi \gg 1$, and

$$f = 2\nu_{\mathrm{av}}/\nu_f \qquad (D19)$$

if $fi \gg 1$. It is easily seen that the former case corresponds to the situation of high stresses and the latter to that of low stresses.

In the case $fi \ll 1$, $f_l(p)$ and $f_r(p)$ change little from segment to segment; that is, kinks are quite uniformly distributed on a dislocation. On the other hand, kinks collide with the opposite kind of kinks near the middle of two adjacent active segments, if $fi \gg 1$.

The dislocation velocity is given by:

$$v = \left(a \Big/ \sum_{p=-\infty}^{+\infty} l_p\right) \left\{ \sum_{p=-\infty}^{+\infty} \sum_{q=p+1}^{+\infty} \nu_q F_l(q,p) l_p \right.$$

$$\left. + \sum_{p=-\infty}^{+\infty} \sum_{q=-\infty}^{p-1} \nu_q F_r(q, p+1) l_p + \sum_{p=-\infty}^{+\infty} \nu_p l_p \right\}$$

$$= \left(a \Big/ \sum_{p=-\infty}^{+\infty} l_p\right) \sum_{p=-\infty}^{+\infty} \left[\frac{\nu_f}{2} f_r(p) + \frac{\nu_f}{2} f_l(p+1) + \nu_p\right] l_p$$

$$= \frac{a\nu_f f}{2} + \frac{2a \sum \nu_p l_p}{\sum l_p} \approx \frac{a\nu_f f}{2}. \qquad (D20)$$

Inserting (D18) and (D19) to (D20) one gets

$$v = (2a\bar{l}\nu_0^* \nu_f{}^0)^{1/2}\left(1 + \frac{E_d}{\tau ab\bar{l}} + \frac{x^*}{\bar{l}}\right)^{1/2}$$

$$\times \exp\left(-\frac{E^* + E_d - \tau abx^*}{2kT} - \frac{E_d}{2\tau ab\bar{l}} - \frac{x^*}{2\bar{l}}\right) \qquad (D21)$$

for the velocity under high stresses, and

$$v = \bar{l}\nu_0^*\left(1 + \frac{E_d}{\tau ab\bar{l}} + \frac{x^*}{\bar{l}}\right) \exp\left(-\frac{E^* - \tau abx^*}{kT}\right) \qquad (D22)$$

for low stresses.

Equation (D22) shows a much weaker dependence on stress than (D21). When one plots the velocity against $1/\tau$, one has Fig. 10(a).

The collision length of kinks is obtained by using Eq. (11) and is given by $\lambda = 2\bar{l}/f$ in the region where the velocity is given by (D21) and by $\lambda = \bar{l}i/2$ in the low-stress region. At the intersecting point of the curves (D21) and (D22), the collision length is $\lambda = \bar{l}/\alpha$ ($\alpha = \nu_{\mathrm{av}}/\nu_f$).

The above discussion is appropriate for a dislocation of infinite length. Actually a dislocation has finite length. Then for a dislocation of length L the velocity is given by Eq. (12) for stresses lower than the stress at which the collision length is $L/2$. Hence, the logarithm of the velocity plotted against $1/\tau$ has a shape shown in Figs. 10(b) and (c) for a dislocation longer and shorter than $2\bar{l}/\alpha$, respectively.